Phonons in single-layer and few-layer MoS_2 and WS_2

A. Molina-Sánchez* and L. Wirtz

Institute for Electronics, Microelectronics, and Nanotechnology (IEMN), CNRS-UMR 8520, Department ISEN, Boîte Postale 60069, F-59652 Villeneuve d'Ascq, France

(Received 28 July 2011; published 11 October 2011)

We report *ab initio* calculations of the phonon dispersion relations of the single-layer and bulk dichalcogenides MoS_2 and WS_2. We explore in detail the behavior of the Raman-active modes A_{1g} and E^1_{2g} as a function of the number of layers. In agreement with recent Raman spectroscopy measurements [C. Lee *et al.*, ACS Nano **4**, 2695 (2010)], we find that the A_{1g} mode increases in frequency with an increasing number of layers while the E^1_{2g} mode decreases. We explain this decrease by an enhancement of the dielectric screening of the long-range Coulomb interaction between the effective charges with a growing number of layers. This decrease in the long-range part overcompensates for the increase of the short-range interaction due to the weak interlayer interaction.

DOI: 10.1103/PhysRevB.84.155413 PACS number(s): 63.10.+a, 63.20.dk, 71.15.Mb

I. INTRODUCTION

Recently, the mechanical exfoliation technique, applied to layered materials, has lead to the fabrication of unique bidimensional systems, i.e., atomically thin layers.[1] Graphene,[2] a planar sheet of carbon atoms arranged in a hexagonal lattice, is the most well-known bidimensional material and exhibits physical properties not found in its bulk counterpart graphite.[3,4] However, the absence of a band gap makes its use in electronic devices (transistors) difficult. Several strategies have been proposed to overcome this setback by opening a gap: quantum confinement in nanoribbons,[5] deposition of a graphene monolayer on boron nitride,[6] applying an electric field in bilayer graphene,[7] etc. Nevertheless, the experimental realization of a band gap larger than 400 meV remains a challenge,[8] as well as a deterioration of other graphene properties, in particular, the high mobility. Therefore, the fabrication of atomically thin sheets of other materials, with a finite band gap, appears to be the natural strategy in the search for materials for another generation of electronic devices.

In recent experiments, molybdenum disulfide (MoS_2), an indirect semiconductor of band gap 1.29 eV in its bulk phase, has exhibited a direct band gap of 1.75 eV in its single-layer phase, together with an enhancement of the luminescence quantum yield in comparison with the MoS_2 bulk.[9,10] Moreover, Radisavljevic *et al.*[11] have demonstrated suitable properties of a single-layer MoS_2-based transistor, such as a room-temperature electron mobility close to that of graphene nanoribbons and a high on/off ratio. Therefore, single-layer MoS_2 has become an appealing material in the area of optoelectronic devices, being an alternative and/or complement to graphene. From other layered compounds such as WS_2, MoS_2, BN, etc., monolayers can be produced by (liquid) exfoliation as well.[12] Moreover, MoS_2 and other layered materials are also interesting due to the change of certain properties with respect to their bulk counterparts. Finally, their topology facilitates atom-by-atom chemical identification.[13]

Recent Raman spectroscopy measurements of single-layer and multilayer MoS_2 have revealed unexpected trends of the vibrational properties when the number of layers changes. Lee *et al.*[14] reported a decrease in frequency of the optical E^1_{2g} phonon mode with increasing numbers of layers. This is consistent with the finding that in bulk MoS_2 the infrared-active E_{1u} mode (where neighboring layers are vibrating in phase) is slightly lower in frequency than the Raman-active E^1_{2g} mode (where neighboring layers are vibrating with a phase shift of π).[15] But both observations contradict the naive expectation that the weak interlayer forces should increase the effective restoring forces acting on atoms. One would thus rather expect a slight increase of the frequency of the Raman-active mode with respect to the IR-active mode[16] and, accordingly, an increase of the frequency of the bulk Raman-active mode with respect to the corresponding single-layer mode. As a plausible explanation of this anomalous trend the long-range Coulomb interaction was mentioned.[14] The purpose of our paper is the clarification of this issue by a detailed *ab initio* study of the interatomic force constants, separating the short-range and the long-range Coulomb parts. We show in the following that the anomalous trend in the E^1_{2g} mode frequency is caused by the dielectric screening of the long-range Coulomb forces in bulk MoS_2. At the same time, we present a full *ab initio* study of the phonon dispersion relations of single-layer and of bulk MoS_2 and the intimately related material WS_2. (Tungsten is in the same column of the periodic system as molybdenum.) Apart from a study of the vibrational stability of MoS_2 nanoribbons,[17] to the best of our knowledge, a fully comprehensive *ab initio* study of the vibrational properties of these materials is still absent in the literature.

In Sec. II we present the methods for the calculation of the phonon dispersions and the analysis of the force constants. In Sec. III we discuss the phonon dispersion relations of MoS_2 and WS_2 single layers and bulk and compare them with experimental data. In Sec. IV, we present the calculated results for the evolution of the Raman-active phonon modes as a function of the number of layers and give an explanation in terms of the short-range and long-range contributions to the force constants.

II. CALCULATION METHODS

MoS_2 and WS_2 belong to the dichalcogenide family of materials, built up of weakly bonded S-Mo-S single layers as shown in Fig. 1. Each one of these single layers consists

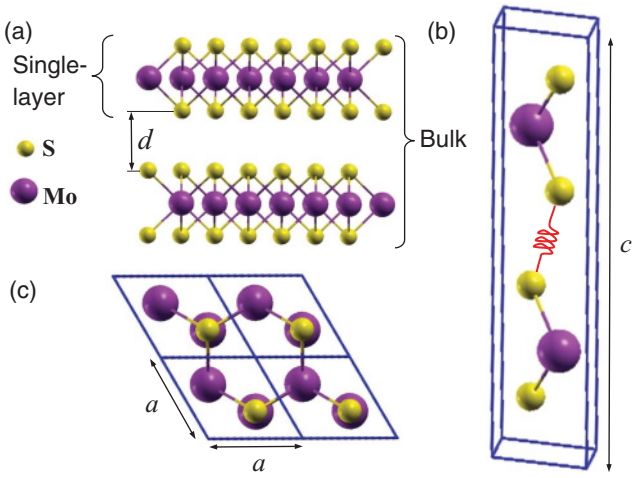

FIG. 1. (Color online) (a) MoS_2 bulk and single layer. The interlayer distance is denoted by d. (b) and (c) Slide and top view of the MoS_2 bulk unit cell (analogous for WS_2). The primitive vectors are $\boldsymbol{a} = (a,0,0)$, $\boldsymbol{b} = (a/2,\sqrt{3}a/2,0)$, and $\boldsymbol{c} = (0,0,c)$. The weak layer interaction is indicated by a spring.

of two hexagonal planes of S atoms and an intercalated hexagonal plane of Mo atoms bound with the sulfur atoms in a trigonal prismatic arrangement. The symmetry space group of bulk MoS_2 is $P3m1$ (point group D_{6h}). The space group of the single layer is $P6m2$ (point group D_{3h}). Consequently, systems with even numbers of layers belong to the space group $P3m1$ (with inversion symmetry), and systems with odd numbers of layers to the $P6m2$ space group (without inversion symmetry).

The phonon calculations begin with the determination of the equilibrium geometry (i.e., the relative atomic positions in the unit cell which yield zero forces and the lattice constants which lead to a zero-stress tensor). The calculations have been done with density functional theory (DFT) as implemented in the open-source code ABINIT,[18] within the local density approximation (LDA).[19] We use Hartwigsen-Goedecker-Hutter pseudopotentials[20] (including the semicore electrons as valence electrons in the case of Mo and W) and a plane-wave cutoff at 60 Ha. The first Brillouin zone is sampled with a $12 \times 12 \times 4$ Monkhorst-Pack grid for bulk and $12 \times 12 \times 1$ for single-layer and few-layer systems.

The optimized lattice parameters are shown in Table I. The experimental lattice parameters of MoS_2 are $a = 3.15$ and $c = 12.3$ Å.[21] In the case of WS_2 they are $a = 3.153$ and $c = 12.323$ Å.[22] Our LDA calculations underestimate them by 0.7% and 2.1%, respectively. The slight underestimations of the in-plane lattice constant are a common feature of the LDA, which tends to overestimate the strength of covalent bonds. For the single layer, we checked the influence of the exchange-correlation potential on the geometry and the phonon dispersion by performing calculations within the generalized gradient approximation (GGA).[23] For the single layers of both MoS_2 and WS_2, we obtain a lattice constant $a = 3.18$ Å, 1.76% larger than the LDA value and 0.96% larger than the experimental (bulk) value. Correspondingly, the phonon frequencies are reduced by an almost constant factor of 1.04% throughout the whole phonon dispersion.

TABLE I. Equilibrium lattice parameters of MoS_2 and WS_2 obtained in this paper.

Lattice constants (Å)			
MoS_2	One layer	Two layers	Bulk
a	3.125	3.126	3.127
c	–	–	12.066
WS_2	One layer	Two layers	Bulk
a	3.125	3.125	3.126
c	–	–	12.145

The correct description of the c parameter is less evident because the LDA (and other semilocal functionals) completely neglect the van der Waals component of the interlayer interaction. At the same time, however, the LDA strongly overestimates the (weak) covalent part of the interlayer bonding. Thus, the LDA has quite successfully reproduced the geometry and also given reasonable results for layer phonon modes of different layered materials such as graphite[24] and hexagonal boron nitride (hBN),[25] as well as of single layers of hBN (Ref. 26) and graphene[27] on a Ni(111) surface. We thus expect (and the obtained value for c supports this expectation) that the LDA works reasonably well for the interlayer phonons of the MoS_2. We note that a physically correct description of the equilibrium geometry, and the potential energy surface around it, would require the proper treatment of the van der Waals contribution, e.g., on the level of the random-phase approximation as it has been done for bulk hBN (Ref. 28) and for graphite.[29] Alternatively, nonlocal functionals that are optimized for the description of the van der Waals interaction[30] could be used. Both approaches are, however, out of the scope of the present paper.

For the calculations of single-layer and few-layer systems, we have used a periodic supercell, leaving enough distance between adjacent sheets. For instance, we use $c = 13.25$ Å in the case of a single layer. The remaining interlayer interaction has negligible effects on the phonon frequencies. All the results show a slight reduction of the in-plane lattice constant, together with a slight stretching of the vertical distances, with the total effect of a smaller Mo-S bond length for decreasing numbers of layers, being 2.382 Å for a single layer and 2.384 Å for bulk MoS_2.

Once the equilibrium geometry has been obtained, the phonon frequencies ω can be calculated. These phonon frequencies are the solution of the secular equation

$$\left| \frac{1}{\sqrt{M_I M_J}} \tilde{C}_{I\alpha,J\beta}(\boldsymbol{q}) - \omega^2(\boldsymbol{q}) \right| = 0, \tag{1}$$

where $\boldsymbol{q}$ is the phonon wave vector, and M_I and M_J are the atomic masses of atoms I and J. The dynamical matrix is then defined as

$$\tilde{C}_{I\alpha,J\beta}(\boldsymbol{q}) = \frac{\partial^2 E}{\partial u_I^{*\alpha}(\boldsymbol{q}) \partial u_J^{\beta}(\boldsymbol{q})}, \tag{2}$$

where $u_I^{\alpha}(\boldsymbol{q})$ denotes the displacement of atom I in direction α. The second derivative of the energy in Eq. (2) corresponds

to the change of the force acting on atom I in direction α with respect to a displacement of atom J in direction β:[31]

$$\tilde{C}_{I\alpha,J\beta}(\boldsymbol{q}) = -\frac{\partial F_I^\alpha}{\partial u_J^\beta(\boldsymbol{q})}. \quad (3)$$

The Fourier transform of the $\boldsymbol{q}$-dependent matrix leads to the real-space atomic force constant matrix $C_{I\alpha,J\beta}(\boldsymbol{R}_{IJ})$, where $\boldsymbol{R}_{IJ}$ is the vector that joins atoms I and J. Thus, $C_{I\alpha,J\beta} < 0\ (>0)$ means a binding (antibinding) force in direction α acting on atom I when atom J is displaced in direction β. It is worth mentioning that the diagonal term in the atom index $C_{I\alpha,I\beta}$ corresponds, according to Newton's third law, to the total force exerted on atom I in direction α upon displacement of all other atoms in direction β:[32]

$$C_{I\alpha,I\beta}(\boldsymbol{0}) = \sum_{J\neq I}^{\infty} \frac{\partial F_I^\alpha}{\partial u_J^\beta}. \quad (4)$$

This term is always positive (unless the crystal is unstable) and in the following we refer to it as self-interaction. Equation (4) demonstrates the contribution of many atoms to the self-interaction. One can distinguish two contributions, the short-range part (which is mainly due to covalent bonding to the close neighbors) and the Ewald or long-range part[33] (due to the Coulomb forces between the effective charges). This distinction will be helpful to interpret the evolution of the self-interaction for varying layer thicknesses and to understand the unexpected trends of the phonon frequencies (Sec. IV).

For the calculation of the dynamical matrix we have used density functional perturbation theory (DFPT)[31] where atomic displacements are taken as a perturbation potential, and the resulting changes in electron density and energy are calculated self-consistently through a system of Kohn-Sham-like equations. Within this approach the phonon frequency can be obtained for arbitrary $\boldsymbol{q}$, with calculation only in a single unit cell.

Since MoS_2 and WS_2 are slightly polar materials, certain IR-active phonon modes at Γ give rise to a macroscopic electric field. This electric field affects the longitudinal optical (LO) phonons in the limit $\boldsymbol{q} \to 0$, breaking the degeneracy of the LO mode with the transversal optical (TO) mode.[34] Thus, in bulk MoS_2 and WoS_2, the nonanalytic part of the dynamical matrix (which contains the effective charges and the dielectric tensor) must be calculated in order to obtain the correct frequencies at the Brillouin zone center.[35] The LO-TO splitting for the E_{1u} mode has the value of 2.8 cm^{-1}. In the case of a single-layer or few-layer system, this effect is even smaller.

III. PHONON DISPERSIONS

A. MoS_2

We start our analysis of the vibrational properties with the description of the general features of the phonon dispersions of bulk and single-layer MoS_2, shown in Fig. 2. We have also depicted the experimental data obtained with neutron inelastic scattering spectroscopy.[21] The overall agreement between theory and experiment is good, even for the interlayer modes. This confirms our expectation that the LDA describes reasonably well the interlayer interaction (even though it does not describe the proper physics of the interlayer forces).

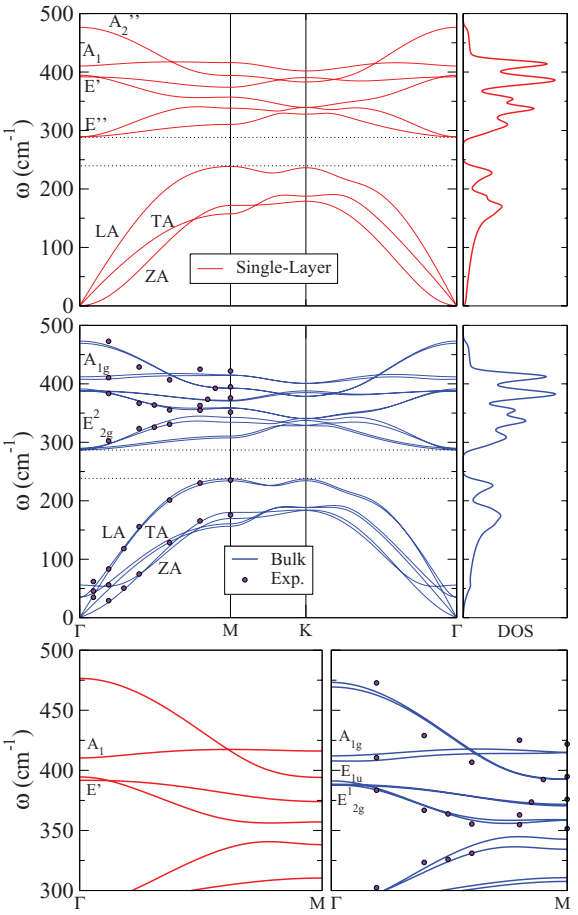

FIG. 2. (Color online) Phonon dispersion curves and density of states of single-layer and bulk MoS_2. Points are experimental data extracted from Ref. 21. Bottom panel: Inset of the phonon branches in the region of the E^1_{2g} and A_{1g} modes.

The bulk phonon dispersion has three acoustic modes. Those that vibrate in-plane [longitudinal acoustic (LA) and transverse acoustic (TA)] have a linear dispersion and higher energy than the out-of-plane acoustic (ZA) mode. The latter displays a q^2 dependence analogous to that of the ZA mode in graphene (which is a consequence of the point-group symmetry[36]). The low-frequency optical modes are found at 35.2 and 57.7 cm^{-1} and correspond to rigid-layer shear and vertical motion, respectively (analogous with the low-frequency optical modes in graphite[37]). When the wave number $\boldsymbol{q}$ increases, the acoustic and low-frequency optical branches almost match. It is worth mentioning the absence of degeneracies at the high-symmetry points M and K and the two crossings of the LA and TA branches just before and after the M point.

The high-frequency optical modes are separated from the low-frequency modes by a gap of 49 cm^{-1}. We have drawn in Fig. 3 the atomic displacements of the Raman-active modes E^1_{2g} and A_{1g} and the infrared-active mode E_{1u}. The Raman-active modes are also indicated in the phonon dispersion of Fig. 2. The in-plane modes E^1_{2g} and E_{1u} are slightly split in

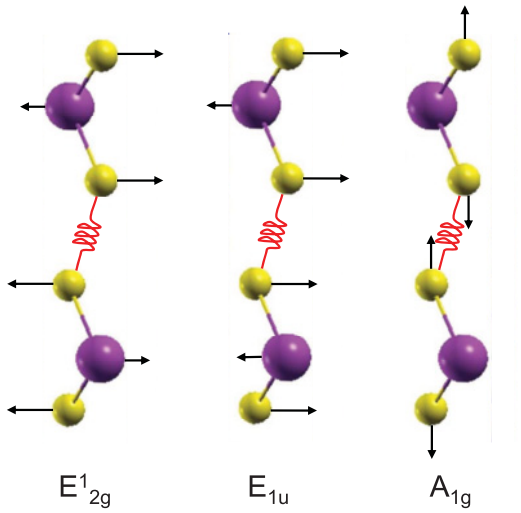

FIG. 3. (Color online) In-plane phonon modes E^1_{2g} and E_{1u}, and the out-of-plane phonon mode A_{1g}, for the bulk MoS_2 (analogously for WS_2).

energy (by 3 cm^{-1}). This is known as Davydov splitting and, for MoS_2, the experimental value is 1 cm^{-1}.[15] However, the finding that the E_{1u} frequency is larger than that of the E^1_{2g} mode contradicts *a priori* what one would expect from the weak interlayer interaction: As one can see in Fig. 3, for the E^1_{2g} mode, the sulfur atoms of different layers move in opposite direction and thus the additional "spring" between sulfur atoms of neighboring layers should increase the frequency of the E^1_{2g} mode with respect of that of the E_{1u} mode, where sulfur atoms of neighboring sheets are moving in phase and thus the additional "spring" has no effect. The semiempirical model of Ref. 16 takes this consideration into account, and obtained indeed that $\omega_{E^1_{2g}} > \omega_{E_{1u}}$, while experiments in Refs. 15 and 16 demonstrate the opposite behavior. Our *ab initio* calculations match the experimental results, which indicates that other causes beyond the weak interlayer interaction are present in the system. We will analyze this feature in the next section with the aid of the atomic force constants.

We now turn to analyze the single-layer phonon dispersion, shown in Fig. 2. The symmetry is reduced from D_{6h} to D_{3h} and there is no longer a center of inversion as in the bulk. Therefore, the phonon mode labels at Γ must be changed accordingly. The number of phonon branches is reduced to nine. Table II shows the most relevant MoS_2 single-layer and bulk modes at Γ, together with their character, displacement direction, involved atoms, and frequency.

Overall, the single-layer and bulk phonon dispersions share a resemblance. In the bulk, all single-layer modes are split into two branches, but since the interlayer interaction is weak, the splitting is very low (similar to the situation in graphite and graphene.[37] The only notable exception from this is the splitting of the acoustic modes around Γ. In the single layer, the resulting low-frequency optical modes are absent.

In the single layer, the high-frequency Γ modes E^1_{2g} and E_{1u} collapse into the mode E'. (From Fig. 3 it is evident that with increasing interlayer distance, the modes E^1_{2g} and E_{1u} acquire the same frequency.) Interestingly, as measured in Ref. 14 and indicated in Table II, the bulk E_{2g} mode is lower in frequency

TABLE II. Relevant phonon symmetry representations of single-layer (point group D_{3h}) and bulk (point group D_{6h}) MoS_2 (inspired by Table II of Ref. 15). Direction out of plane (in plane) is parallel (perpendicular) to the $\boldsymbol{c}$ vector of the unit cell, respectively. Phonon frequencies are the calculated values of this paper.

D_{3h}	D_{6h}	Character	Direction	Atoms	ω_{MoS_2} (cm^{-1})	
A_2	A_{2u}	Acoustic	Out of plane	Mo + S	0.0	0.0
	B^2_{2g}	Inactive	Out of plane	Mo + S	–	55.7
–	E^2_{2g}	Raman	In plane	Mo + S	–	35.2
A_1	A_{1g}	Raman	Out of plane	S	410.3	412.0
	B_{1u}	Inactive	Out of plane	S		407.8
A''_2	A_{2u}	Infrared ($\boldsymbol{E}\|\|\boldsymbol{c}$)	Out of plane	Mo + S	476.0	469.4
	B^1_{2g}	Inactive	Out of plane	Mo + S		473.2
E'	E^1_{2g}	Raman	In plane	Mo + S	391.7	387.8
	E_{1u}	Infrared ($\boldsymbol{E}\perp\boldsymbol{c}$)	In plane	Mo + S		391.2
E''	E_{1g}	Raman	In plane	S	289.2	288.7
	E_{2u}	Inactive	In plane	S		287.1

than the single-layer E' mode. This contradicts the expectation that the additional interlayer interaction should increase the frequency but is in line with the anomalous sign of the Davydov splitting between the bulk E^1_{2g} and E_{1u} modes. The origin of this will be discussed in Sec. IV. The out-of-plane mode A_{1g} follows the expected trend that the interlayer interaction increases the frequency with respect to the single-layer mode A_1.

The densities of states (DOS) of the single-layer and bulk modes are represented in the right-hand panels of Fig. 3. The differences between single-layer and bulk DOS are minimal, except for a small shoulder ∼60 cm^{-1} in the bulk DOS due to the low-frequency optical modes. In both cases the highest peaks are located close to the Raman-active modes E^1_{2g} and A_{1g}.

B. WS_2

Figure 4 shows the phonon dispersions of single-layer and bulk WS_2, together with the DOS. The general features are identical to those of the dispersions of MoS_2 (Fig. 2). The differences between single-layer and bulk dispersions are similarly weak as in the case of MoS_2. Thus, the bulk DOS also resembles very much that of the single layer (except for the small shoulder ∼50 cm^{-1} due to the interlayer optical modes).

For a better comparison of MoS_2 and WS_2 single-layer phonon frequencies, we have depicted them together in Fig. 5. In general, the WS_2 phonon bands are shifted down to lower frequencies with respect to the MoS_2 frequencies. The cause of this trend is the larger mass of the tungsten atoms, and therefore their lower vibration frequency [see Eq. (1)]. The only notable exceptions from this general downshift are the branches associated to the E'' mode, ∼300 cm^{-1}, and to the A_1 mode, ∼410 cm^{-1}. In these modes, only the sulfur atoms are vibrating (see Table II) and thus their frequency is not affected by the mass of the metal atom (W or Mo), just by the strength of the covalent bond.

The larger mass of W leads to a larger frequency gap between low- and high-frequency modes (110 cm^{-1}) since

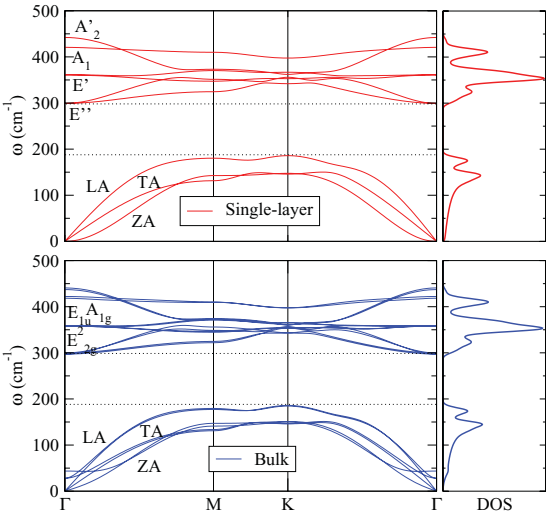

FIG. 4. (Color online) Phonon dispersion curves and density of states of one-layer and bulk WS_2.

the highest acoustic branch is pushed down. Furthermore, the difference between the A_1 and E' modes is now 60 cm^{-1}, three times larger than in the case of MoS_2.

The density of states of the single-layer WS_2 is also appreciably different from that of MoS_2. While at low frequencies the DOS has two well-differentiated peaks, as in Fig. 2, for higher energies one peak stands out from the others, at a frequency of ∼350 cm^{-1}, and is associated mainly with the Γ-point mode E'.

IV. EVOLUTION OF A_{1g} AND E^1_{2g} PHONON MODES WITH THE NUMBER OF LAYERS

The understanding of the frequency trends of the A_{1g} and E_{2g} modes with varying layer thicknesses requires a more refined analysis. With the aim of explaining the Raman scattering experiments of Ref. 14, we have calculated the phonon frequencies at the Γ point for single, double, and triple layers and we discuss the evolution of the atomic force constants from a single layer to bulk in detail.

Figure 6 shows the phonon frequency of A_{1g} and E^1_{2g} modes as a function of the number of layers. Since LDA tends to overestimate the phonon frequencies, it is reasonable to

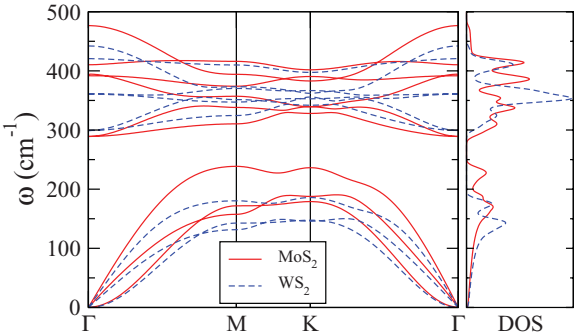

FIG. 5. (Color online) Phonon dispersion curves for single-layer MoS_2 (solid lines) and WS_2 (dashed lines). The density of states is depicted in the right-hand panel.

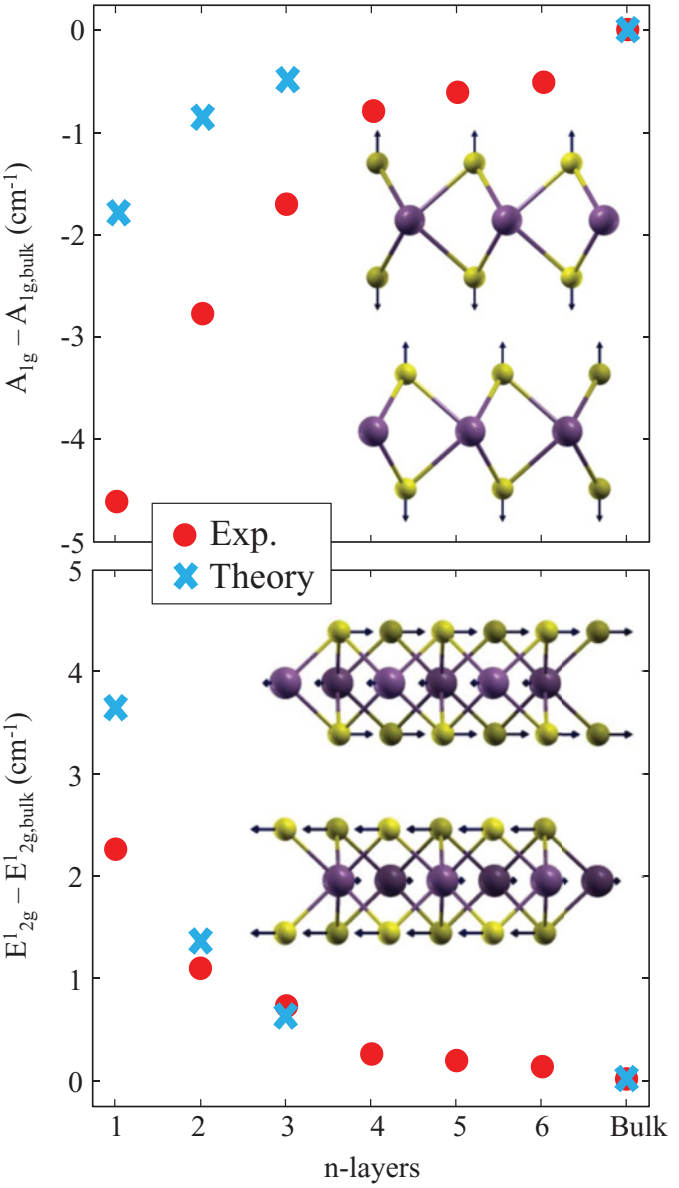

FIG. 6. (Color online) Phonon frequencies of A_{1g} and E^1_{2g} modes as a function of MoS_2 layer thickness, as obtained in this paper (squares) and experimental data from Ref. 14 (circles). We plot the frequency differences with respect to the corresponding bulk modes. The insets represent the phonon modes at Γ point.

represent the difference between the n-layer frequency and the bulk frequency instead of comparing absolute theoretical and experimental values. In such a representation we observe that our calculations properly reproduce the upshift of the A_{1g} mode and the downshift of the E^1_{2g} mode with increasing numbers of layers. The quantitative differences between theory and experiment are mainly due to the limited precision of the description of the interlayer interaction by the LDA.

After we have shown that DFPT-LDA reproduces the experimental trends we would like to give an explanation of this behavior, taking advantage of the detailed knowledge of the atomic force constants, available in *ab initio* methods. We interpret the changes in phonon frequency through an analysis of the real-space force constants [Eq. (3)], in particular, of the

TABLE III. Self-interaction term $C_{S\alpha,S\alpha}$ and $C_{Mo\alpha,Mo\alpha}$ of the Mo and S atoms, and atomic force constants between S atoms of adjacent layers $C_{Sz,S'z}$, as defined in Sec. II (atomic units). The dielectric tensor ϵ of both systems is also given (nondiagonal elements are zero).

	Atom	$C_{Sz,Sz}$	$C_{Sz,S'z}$	$C_{Mox,Mox}$	Long range	Short range	$\epsilon_{xx} = \epsilon_{yy}$	ϵ_{zz}
Bulk	Mo	–	–	0.27660	0.00308	0.27352	15.40	7.43
	S	0.15837	−0.00099	0.12310	0.00071	0.12239		
One layer	Mo	–	–	0.28275	0.01058	0.27217	7.36	1.63
	S	0.15860	–	0.12320	0.00265	0.12055		

self-interaction term [Eq. (4)]. Going from a single layer to a multilayer, this term changes in two ways: (i) The short-range term increases due to the (weak, but non-negligible) interaction with atoms from neighboring layers; and (ii) the long-range Coulomb interaction changes, because the sum extends over effective charges from all layers and the effective screening of the Coulomb potential increases.

We start our analysis with the out-of-plane A_{1g} mode. From Fig. 3, it is intuitively clear that the interaction between sulfur atoms of neighboring layers can substantially influence the frequency. Going from the single layer to the double layer, one "adds" an additional "spring" between the atoms S and S′ on neighboring layers, which leads to an increase of the A_{1g}-mode frequency with increasing number of layers. As only sulfur atoms are involved in this mode, we just need to examine the sulfur self-interaction term ($C_{Sz,Sz}$) and the atomic force constant ($C_{Sz,S'z}$) between nearest neighbors that belong to adjacent layers (atoms joined by the spring in Fig. 3). We have summarized the results in Table III. Note that the small variation of the term $C_{Sz,Sz}$ from a single layer to bulk prevents it from being the main cause of a frequency increase of almost 5 cm^{-1}. Thus, the term $C_{Sz,S'z}$ has a negative value, which implies a binding force ("spring") between atoms S and S′, which leads to an increase of frequency. Force constants related to farther neighbors are negligible in comparison with $C_{Sz,S'z}$. This demonstrates that the weak interlayer interaction is the main cause of the frequency increasing with the number of layers.

One might expect that the same argument holds for the E^1_{2g} mode: The additional "spring" between sulfur atoms from neighboring layers should increase the frequency with increasing number of layers as well. However, theoretical and experimental results show the opposite behavior. The reason can be found in the self-interaction terms $C_{Mox,Mox}$ for Mo and S in Table III: While the difference between the single layer and bulk is negligible for the sulfur atoms, one observes a considerable decrease for the molybdenum atoms. Interestingly, the short-range contribution to the self-interaction increases (as one would expect from the interlayer interaction). However, the long-range Coulomb part[33] decreases considerably. In the Appendix, we show that this decrease is related to the strong increase of the dielectric tensor (both in plane and out of plane) when going from the single layer (represented in our calculations by a periodic stacking of single layers with a large vacuum between) to the bulk (see Table III). We note that one might associate the change in frequency to the differences in the lattice constant and interatomic distances in bulk and the single layer, respectively. However, the small differences shown in Sec. II are not enough to account for the observed magnitude of the E^1_{2g} frequency change.[38]

Therefore, the decrease of the E^1_{2g} phonon frequency is associated with a stronger dielectric screening of the long-range Coulomb interaction in few-layer and bulk MoS_2. The effect is particularly pronounced for the molybdenum atoms, as Table III shows. Our analysis also explains why previous empirical models have not been able to explain the experimental observations, due to the difficulty of including this subtle change in the parameters.

V. CONCLUSIONS

In conclusion, we have studied the phonon dispersions of MoS_2 and WS_2 single layers and bulk using density functional perturbation theory in the local density approximation. We obtain good agreement with neutron diffraction data as well as Raman and infrared absorption spectroscopies. We have explored how the Raman-active modes A_{1g} and E^1_{2g} change in frequency when the number of layers varies, and confirm the recently reported downshift of the E^1_{2g} mode with increasing numbers of layers. This unexpected behavior can be explained by an increase of the dielectric screening which reduces the long-range Coulomb interaction between the effective charges and thus reduces the overall restoring force on the atoms. We expect that this explanation also holds for other polar layered materials where an anomalous Davydov splitting has been observed [such as GaSe (Ref. 39) and GaS (Ref. 40)].

ACKNOWLEDGMENTS

Funding was provided by the French National Research Agency (ANR) through Proj. No. bl-inter09_482166. Calculations were done at the IDRIS supercomputing center, Orsay (Proj. No. 091827).

APPENDIX

The examination of the long-range atomic force constant formula can help to establish quantitatively its change with the variation of the dielectric tensor in single-layer and bulk MoS_2. However, the anisotropy of the crystalline structure of MoS_2 impedes a direct relationship between the long-range atomic force constants and the dielectric tensor. The long-range contribution $C^{lr}_{I\alpha,J\beta}$ can be written in terms of the dielectric

tensor $\boldsymbol{\epsilon}$, its inverse, $\boldsymbol{\epsilon}^{-1}$, the Born effective charges $Z^*_{I,\alpha\alpha'}$, and the interatomic distance $\boldsymbol{d} \equiv \boldsymbol{d}_{IJ}$, as defined in Ref. 33:

$$C^{\rm lr}_{I\alpha,J\beta} = \sum_{\alpha',\beta'} Z^*_{I,\alpha,\alpha'} Z^*_{J,\beta,\beta'} \left[\frac{(\epsilon^{-1})_{\alpha'\beta'}}{D^3} - 3\frac{\Delta_{\alpha'}\Delta\beta'}{D^5} \right] \times (det\epsilon)^{-1/2},$$

where $\Delta_\alpha = \sum_\beta (\boldsymbol{\epsilon}^{-1})_{\alpha\beta} d_\beta$ is the conjugate of the vector $\boldsymbol{d}$, and the norm of the latter in this metrics is $D = \sqrt{\boldsymbol{\Delta}\cdot\boldsymbol{d}}$. This expression simplifies enormously by assuming a diagonal dielectric tensor, and $Z^*_{I,\alpha\alpha'} \equiv Z^*_{I,\alpha\alpha'}\delta_{\alpha\alpha'}$. After some algebra one obtains

$$C^{\rm lr}_{I\alpha,J\beta} = \frac{Z^*_{I,\alpha\alpha} Z^*_{J,\beta\beta}}{\sqrt{\epsilon_{xx}\epsilon_{yy}\epsilon_{zz}}} \left(\frac{\epsilon^{-1}_{\alpha\beta}\delta_{\alpha\beta}}{D^3} - 3\frac{\epsilon^{-1}_{\alpha\alpha}\epsilon^{-1}_{\beta\beta} d_\alpha d_\beta}{D^5} \right). \quad \text{(A1)}$$

We can examine with an example how the long-range atomic force constants of single-layer and bulk MoS_2 are related with the dielectric tensors. Thus, we can evaluate the term $C^{\rm lr}_{I\alpha,J\beta}$ for neighbor Mo atoms that belong to the same layer, with interatomic distance $\boldsymbol{d} = (d,0,0)$, and assuming the same distance for the single layer and the bulk. Thus, we obtain a simplified expression of Eq. (A1):

$$C^{\rm lr}_{{\rm Mo},x,{\rm Mo},x} = -2\frac{(Z^*_{{\rm Mo},xx})^2}{\sqrt{\epsilon_{xx}\epsilon_{zz}}d^3}. \quad \text{(A2)}$$

The Born effective charges $Z^*_{{\rm Mo},xx}$ are almost equal for both systems, and using the dielectric tensors given in Table III, we obtain

$$\frac{C^{\rm lr}_{{\rm Mo},x,{\rm Mo},x}(1l)}{C^{\rm lr}_{{\rm Mo},x,{\rm Mo},x}({\rm bulk})} = \sqrt{\frac{\epsilon_{xx,{\rm bulk}}\epsilon_{zz,{\rm bulk}}}{\epsilon_{xx,1l}\epsilon_{zz,1l}}} = 3.09. \quad \text{(A3)}$$

From the *ab initio* calculation of the atomic constants we obtain $C^{\rm lr}_{{\rm Mo},x,{\rm Mo},x}(1l)/C^{\rm lr}_{{\rm Mo},x,{\rm Mo},x}({\rm bulk}) = 3.19$, which is in agreement with the value obtained in Eq. (A3). This demonstrates that the difference in the long-range part of the force constants for the single-layer and the bulk originates from the different dielectric screening.

*alejandro.molina@isen.iemn.univ-lille1.fr

[1] K. S. Novoselov, D. Jiang, F. Schedin, T. J. Booth, V. V. Khotkevich, S. V. Morozov, and A. K. Geim, Proc. Natl. Acad. Sci. USA **102**, 10451 (2005).

[2] K. S. Novoselov, A. K. Geim, S. V. Morozov, D. Jiang, Y. Zhang, S. V. Dubonos, I. V. Grigorieva, and A. A. Firsov, Science **306**, 666 (2004).

[3] P. R. Wallace, Phys. Rev. **71**, 622 (1947).

[4] A. K. Geim and K. S. Novoselov, Nat. Mater. **6**, 183 (2007).

[5] Y.-W. Son, M. L. Cohen, and S. G. Louie, Phys. Rev. Lett. **97**, 216803 (2006).

[6] G. Giovannetti, P. A. Khomyakov, G. Brocks, P. J. Kelly, and J. van den Brink, Phys. Rev. B **76**, 073103 (2007).

[7] Y. Zhang, T.-T. Tang, C. Girit, Z. Hao, M. C. Martin, A. Zettl, M. F. Crommie, Y. R. Shen, and F. Wang, Nature (London) **459**, 820 (2009).

[8] M. Y. Han, B. Ozyilmaz, Y. Zhang, and P. Kim, Phys. Rev. Lett. **98**, 206805 (2007).

[9] A. Splendiani, L. Sun, Y. Zhang, T. Li, J. Kim, C.-Y. Chim, G. Galli, and F. Wang, Nano Lett. **10**, 1271 (2010).

[10] K. F. Mak, C. Lee, J. Hone, J. Shan, and T. F. Heinz, Phys. Rev. Lett. **105**, 136805 (2010).

[11] B. Radisavljevic, A. Radenovic, J. Brivio, V. Giacometti, and A. Kis, Nat. Nano. **6**, 147 (2011).

[12] J. N. Coleman, M. Lotya, A. O'Neill, S. D. Bergin, P. J. King, U. Khan, K. Young, A. Gaucher, S. De, R. J. Smith, I. V. Shvets, S. K. Arora, G. Stanton, H.-Y. Kim, K. Lee, G. T. Kim, G. S. Duesberg, T. Hallam, J. J. Boland, J. J. Wang, J. F. Donegan, J. C. Grunlan, G. Moriarty, A. Shmeliov, R. J. Nicholls, J. M. Perkins, E. M. Grieveson, K. Theuwissen, D. W. McComb, P. D. Nellist, and V. Nicolosi, Science **331**, 568 (2011).

[13] O. L. Krivanek, M. F. Chisholm, V. Nicolosi, T. J. Pennycook, G. J. Corbin, N. Dellby, M. F. Murfitt, C. S. Own, Z. S. Szilagyi, M. P. Oxley, S. T. Pantelides, and S. J. Pennycook, Nature (London) **464**, 571 (2010).

[14] C. Lee, H. Yan, L. E. Brus, T. F. Heinz, J. Hone, and S. Ryu, ACS Nano **4**, 2695 (2010).

[15] T. J. Wieting and J. L. Verble, Phys. Rev. B **3**, 4286 (1971).

[16] P. N. Ghosh and C. R. Maiti, Phys. Rev. B **28**, 2237 (1983).

[17] C. Ataca, H. Sahin, E. Aktürk, and S. Ciraci, J. Phys. Chem. C **115**, 3934 (2011).

[18] X. Gonze, J.-M. Beuken, R. Caracas, F. Detraux, M. Fuchs, G.-M. Rignanese, L. Sindic, M. Verstraete, G. Zérah, F. Jollet, M. Torrent, A. Roy, M. Mikami, Ph. Ghosez, J.-Y. Raty, and D. C. Allan, Comput. Mater. Sci. **25**, 478 (2002). The ABINIT code results from a common project of the Université Catholique de Louvain, Corning Incorporated, and other collaborators (http://www.abinit.org).

[19] W. Kohn and L. J. Sham, Phys. Rev. **140**, A1133 (1965).

[20] C. Hartwigsen, S. Goedecker, and J. Hutter, Phys. Rev. B **58**, 3641 (1998).

[21] N. Wakabayashi, H. G. Smith, and R. M. Nicklow, Phys. Rev. B **12**, 659 (1975).

[22] W. J. Schutte, J. L. de Boer, and F. Jellinek, J. Solid State Chem. **70**, 207 (1987).

[23] J. P. Perdew, K. Burke, and M. Ernzerhof, Phys. Rev. Lett. **77**, 3865 (1996).

[24] G. Kresse, J. Furthmüller, and J. Hafner, Europhys. Lett. **32**, 729 (1995).

[25] G. Kern, G. Kresse, and J. Hafner, Phys. Rev. B **59**, 8551 (1999).

[26] J. Serrano, A. Bosak, R. Arenal, M. Krisch, K. Watanabe, T. Taniguchi, H. Kanda, A. Rubio, and L. Wirtz, Phys. Rev. Lett. **98**, 095503 (2007).

[27] A. Allard and L. Wirtz, Nano Lett. **10**, 4335 (2010).

[28] A. Marini, P. Garcia-Gonzalez, and A. Rubio, Phys. Rev. Lett. **96**, 136404 (2006).

[29] S. Lebègue, J. Harl, Tim Gould, J. G. Angyán, G. Kresse, and J. F. Dobson, Phys. Rev. Lett. **105**, 196401 (2010).

[30] H. Rydberg, M. Dion, N. Jacobson, E. Schröder, P. Hyldgaard, S. I. Simak, D. C. Langreth, and B. I. Lundqvist, Phys. Rev. Lett. **91**, 126402 (2003).

[31]S. Baroni, S. de Gironcoli, A. Dal Corso, and P. Giannozzi, Rev. Mod. Phys. **73**, 515 (2001).
[32]P. Brüesch, *Phonons: Theory and Experiments I* (Springer-Verlag, Berlin, 1982).
[33]X. Gonze and C. Lee, Phys. Rev. B **55**, 10355 (1997).
[34]M. Cardona and P. Y. Yu, *Fundamentals of Semiconductors* (Springer-Verlag, Berlin, 1996).
[35]P. Giannozzi, S. de Gironcoli, P. Pavone, and S. Baroni, Phys. Rev. B **43**, 7231 (1991).
[36]R. Saito, G. Dresselhaus, and M. S. Dresselhaus, *Physical Properties of Carbon Nanotubes* (Imperial College Press, London, 1998).
[37]L. Wirtz and A. Rubio, Solid State Commun. **131**, 141 (2004).
[38]In order to proof this hypothesis, we have also examined the frequencies of a single layer, setting bulk interatomic distances in order to mimic as much as possible the bulk environment onto the single layer. The E^1_{2g} is now 390.3 cm^{-1}, which is still larger than the bulk, with a value of 387.8 cm^{-1}. Therefore, we can neglect the distinct interatomic distances as the main cause of the E^1_{2g} frequency trend.
[39]T. J. Wieting and J. L. Verble, Phys. Rev. B **5**, 1473 (1972).
[40]N. Kuroda and Y. Nishina, Phys. Rev. B **19**, 1312 (1979).